Journal of Materials Chemistry A

ROYAL SOCIETY OF CHEMISTRY

REVIEW

View Article Online
View Journal | View Issue



Cite this: J. Mater. Chem. A, 2024, 12, 18866

# Metal–support interactions of 2D carbon-based heterogeneous catalysts for the hydrogen evolution reaction

Weihang Feng,†[a] Wei Zhang, †[a] Quanying Lin,[a] Heshuang Zhang,[a] Jingyuan Qiao,[a] Linhong Xia,[a] Nosipho Moloto, [b] Wei He *[a] and Zhengming Sun *[a]

As research on metal catalytic centers and catalyst supports advances, the interactions (metal–support interactions, MSIs) between them have garnered significant attention. For 2D carbon materials, the inert surface and absence of direct loading sites limit the direct enhancement of catalyst supports. However, further investigation into the optimization and promotion of MSI, including *via* doping heteroatoms and functional groups onto carbon surfaces between the 2D carbon support and metal active centers, which facilitates the uniform dispersion of active metal sites, induces rearrangement of atoms on high-energy crystal planes, and establishes efficient electron transfer pathways to accelerate electron transfer across interfaces, has resulted in outstanding HER performance. In this review, the preparation approaches and the effective carbon surface chemical treatment of 2D carbon-based heterogeneous catalysts are presented. Additionally, a thorough analysis of MSI effects including dispersion of metal active sites, establishment of electron transfer pathways, and electronic structure regulation by lattice strain is discussed in detail. Moreover, personal insights into the prospects and challenges associated with MSI in enhancing HER performance on the 2D carbon matrix are also presented.

Received 28th March 2024
Accepted 12th June 2024

DOI: 10.1039/d4ta02079k

rsc.li/materials-a



## 1 Introduction

In recent times, the critical challenges of the global energy crisis and environmental pollution have required the adoption of eco-friendly, renewable energies, including hydroelectric, hydrogen, solar, and wind power.[1–5] Among these sources, hydrogen exhibits remarkable energy density with zero carbon emission, and electrochemical water splitting has emerged as a promising solution for producing ultrapure hydrogen.[6–10] However, the large-scale application of water electrolysis faces the challenge of requiring a substantial overpotential during the cathodic hydrogen evolution reaction (HER).[11–13] Therefore, the success of large-scale electrocatalytic hydrogen production depends crucially on the characteristics of the catalysts.[14–16] Metal active sites on heterogeneous catalysts play a significant role in the HER. Variations in the metal active centers result in diverse changes in the free energy of adsorption and desorption of HER intermediates.[17,18] Consequently, modifying these metal active centers has emerged as a conventional and widespread approach to enhance the performance of the HER.[19]

Meanwhile, extensive research has also been carried out on catalyst supports. Various catalyst supports can alter the surface microenvironment at the interface, thereby enhancing the activity and stability of catalysts. Among many supports, the global interest in graphene since 2004 has led to widespread attention being paid to two-dimensional (2D) carbon nanomaterials.[20,21] The arrangement of carbon atoms in graphene is the same as that of the graphite monatomic layer, which is bonded by $sp^2$ hybrid orbitals.[22] In the cellular layered structure, σ bonds are linked to other carbon atoms to form hexagonal rings. Thus, the pz orbitals are perpendicular to the layer plane of each carbon atom forming large π bonds (similar to those of the benzene ring) throughout the whole layer leading to excellent electrical properties. The outstanding electrical conductivity and large specific surface area prevent metal sites from agglomerating and optimize their electronic structure, enhancing catalytic activity.[23] Following graphene, graphdiyne (GDY) is a novel 2D carbon allotrope with unique properties that make it an attractive matrix for supporting metal catalysts.[24] GDY possesses active carbon triplet bonds with high binding energy when interacting with metal atoms, which provides numerous anchoring sites for the uniform dispersion of metal nano-catalysts.[25] Unlike graphene, which often requires defects or functional groups to anchor metals, GDY naturally offers an abundance of anchoring sites due to its abundant triple

[a]Key Laboratory of Advanced Metallic Materials of Jiangsu Province, School of Materials Science and Engineering, Southeast University, Nanjing, 211189, People's Republic of China. E-mail: weih@seu.edu.cn; zmsun@seu.edu.cn

[b]Molecular Science Institute, School of Chemistry, University of the Witwatersrand, Private Bag 3, Wits 2050, South Africa

† Weihang Feng and Wei Zhang contributed equally to this paper and should be considered as co-first authors.

bonds.[26] The abundant triple bonds of GDY have strong electron-donating ability, allowing them to adsorb metal cations effectively, which can lead to the creation of zerovalent metal atoms through chemical reduction or electrodeposition.[27] The interaction between GDY and metal active sites can prevent the aggregation of metal atoms and modify the electronic structure of the active sites, enhancing catalytic activity.[24] Furthermore, various carbon materials such as g-$C_3N_4$ (ref. 28) and 2D carbon-containing MOFs[29] have been demonstrated to be effective supports for catalytic sites, enhancing the activity of catalysts. These materials are currently the focus of extensive research for both fundamental studies and practical applications.[30–32]

With the deepening of research on metal catalytic centers and catalyst carriers, the relationship between them has garnered significant attention. Metal–support interactions (MSIs), which describe the relationships between metal catalytic centers and supports, determine catalyst performance.[33–35] Previous studies on MSIs have primarily concentrated on metal active sites and metal oxide carriers. Typical MSIs are related to charge transfer, interfacial perimeter, morphology, chemical composition and strong metal–support interaction (SMSI). The MSIs and their importance in catalysis were first introduced by Tauster *et al.* in 1978. They discovered that the adsorption capacity of hydrogen and carbon monoxide on noble metals supported on $TiO_2$ was influenced by the interfacial properties between the metal species and the support. MSIs stabilize the metal on the support and alter the d-band center of the metal sites, which can also perturb the local electronic structure of the support. The change in the chemical state of the metal induced by charge transfer at the interface plays a crucial role in activating reactants and influencing HER catalytic performance.

As research progressed, the researchers found that using 2D carbon materials as a substrate could also activate MSIs, promoting the HER. In general, carbon materials are perceived to exhibit either no MSI or weak MSI with metal active sites due to their inert surface and absence of direct loading sites. However, some specific preparation methods can introduce functional groups and heteroatoms onto the surface of two-dimensional carbon substrates, making 2D carbon supports more active. These functional groups and heteroatoms form connections with the metal active centers, thereby enhancing MSI and consequently boosting HER activity.[36] Wang *et al.* designed nitrogen-doped carbon nanosheet supported RuM (Mo, W, Cr) (RuM/NCN) by an ultrafast microwave approach. The MSIs between nitrogen doped carbon nanosheets and RuMo favor the enhancement of HER performance (72 mV at 10 mA $cm^{-2}$ in 1 M KOH).[37] Xu *et al.* developed an NCS-CoPt catalyst of $CoPt_3$ nanoparticles loaded on N-doped carbon nanosheets, which achieved nanosize-regulation of metal and support stabilization. The high content of pyridinic N on the carbon substrate could benefit the strong interaction between the carbon support and $CoPt_3$ nanoparticles, which directly contributed to its robust HER activity (41 mV at 10 mA $cm^{-2}$ in 0.5 M $H_2SO_4$).[38] Wang *et al.* reported the remarkable activity of Pd nanoparticles by controlling MSI with nitrogen-doped porous carbon (N-PC). The Pd/N-PC catalyst an exhibited ultralow overpotential of 15.5 mV at 10 mA $cm^{-2}$ in 0.5 M $H_2SO_4$.[39] Besides, recent studies reveal that promoting MSIs on 2D carbon-based catalysts can also facilitate HER performance, compared with MSIs on other supports (metal oxides and metal compounds) in Table 1. Regrettably, in the field of 2D carbon materials, many studies often pay attention to their widespread use, without thorough consideration of their MSI effects.[59–61] Therefore, it is crucial to summarize the MSI effects of 2D carbon materials. Supplementing the understanding of the MSI effects on 2D carbon catalysts and their applications in the HER provides critical insights and guidance for the development of both 2D carbon materials and HER catalysis. Additionally, the advancement of MSI in 2D carbon-based support materials for the HER has not received comprehensive attention and discussion. The mechanisms that induce MSI in 2D carbon materials are still unclear, and the impact of MSIs on metal active centers remains poorly understood. Therefore, it is of great significance to provide an overview of recent MSI developments in the field of 2D carbon-based catalysts for the HER.

As shown in Fig. 1, this review illustrates the common preparation approaches of 2D carbon-based heterogeneous catalysts for the HER. The strategies for modulating MSI on the carbon surface such as heteroatom doping and surface functionalization are presented. Besides the support pre-treatment, the MSI effects on metal including distribution of metal active

Table 1 Comparison of the HER performance of non-carbon-based heterogeneous catalysts and 2D carbon-based heterogeneous catalysts with the MSIs

| 2D carbon-based heterogeneous catalysts | $\eta_{10}$ (mV) | Electrolyte | Ref. |
|---|---|---|---|
| Ru@NC/NG | 16 mV | 1 M KOH | 40 |
| Ru NCs/BNG | 14 mV | 1 M KOH | 42 |
| Ru–S/N–C | 10 mV | 1 M KOH | 44 |
| Ru/S-rGO-24 | 14 mV at $\eta_{20}$ | 1 M KOH | 46 |
| Ru/p-NC | 10 mV | 1 M KOH | 48 |
| Ru/AC | 7 mV | 1 M KOH | 50 |
| Ru–NPCN | 11 mV | 1 M KOH | 52 |
| Pt–NPCN | 9 mV | 1 M KOH | 52 |
| Ru NPs/NC-900 | 19 mV | 1 M KOH | 54 |
| CoPt–CoSA@NSC | 23 mV | 1 M KOH | 56 |
| 3%Pd/N-PC-700 | 15 mV | 0.5 M $H_2SO_4$ | 39 |
| **Non-carbon-based heterogeneous catalysts** | **$\eta_{10}$ (mV)** | **Electrolyte** | **Ref.** |
| Pt/CNTs-N + $\alpha MoC_{1-x}$ | 17 mV | 0.5 M $H_2SO_4$ | 41 |
| $Pd_{58}Ni_{42}$/N-TBA-$V_2CT_x$ | 44.1 mV | 0.5 M $H_2SO_4$ | 43 |
| RuSA@$CoP_x$-300 | 18 mV | 1 M KOH | 45 |
| Pt/TiN NRs-2 | 38 mV | 0.5 M $H_2SO_4$ | 47 |
| $NiMoO_x$@CMK-3 | 7 mV | 1 M KOH | 49 |
| MoN-5% Pt | 11.2 mV | 1 M KOH | 51 |
| MoN-10% Pt | 13 mV | 1 M KOH | 51 |
| Ru/P–MoB | 34 mV | 1 M KOH | 53 |
| Ir@$SrIrO_3$-175 | 28 mV | 0.5 M $H_2SO_4$ | 55 |
| Ru SNC/$W_{18}O_{49}$ | 21 mV | 0.5 M $H_2SO_4$ | 57 |
| HTS-RuNCs/TiN | 16.3 mV | 1 M KOH | 58 |

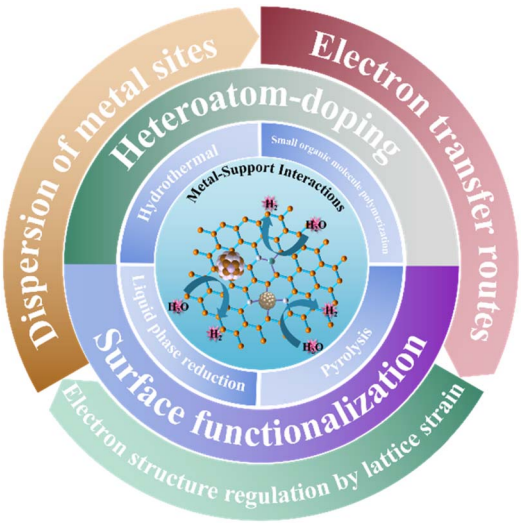


Fig. 1 Illustration of MSI on 2D carbon-based heterogeneous catalysts for the HER.

sites, constructing electron transfer paths and electronic structure regulation by lattice strain engineering are comprehensively discussed. The optimization and enhancement of MSI, including *via* doping heteroatoms and grafting functional groups onto carbon surfaces, facilitate the uniform dispersion of active metal sites and electronic structure regulation by lattice strain, and establish efficient electron transfer pathways to accelerate electron transfer across interfaces, leading to outstanding HER performance. Moreover, the challenges and prospects of MSIs on 2D carbon supports in HER applications are emphasized.

## 2 Preparation approaches of 2D carbon-based heterogeneous catalysts for MSI

The HER is a cathodic half-reaction that can proceed through either the Volmer–Heyrovsky pathway or the Volmer–Tafel pathway in acidic, alkaline and neutral solutions, which are shown in Table 2. In the Volmer reaction, a proton on the catalyst's surface combines with an electron, resulting in the formation of an adsorbed hydrogen (H*) atom as an intermediate.[62,63] Following the Volmer reaction, there are two possible subsequent paths: one involves the amalgamation of an adsorbed H* atom with an electron and a proton (known as the Volmer–Heyrovsky pathway), while the other path is the combination of two H* atoms (referred to as the Volmer–Tafel pathway).[64,65] Hence, it's urgent for highly active 2D carbon-based heterogeneous catalysts to decrease the energy barrier of hydrolysis and tune well the free energy associated with hydrogen adsorption and desorption.[66] Meticulous control during synthesis procedures is imperative to fine-tune the MSI of 2D carbon-based heterogeneous catalysts and optimize their HER performance.[67,68] In this section, we identify four effective approaches to form stable MSI, which could significantly advance the effective HER of 2D carbon-based heterogeneous catalysts under harsh conditions. The relative HER performances and detailed synthesis conditions are summarized in Table 3.

Table 2 Three reaction pathways of the HER under acidic, alkaline and neutral conditions

| Conditions | Step | Pathway |
|---|---|---|
| Acidic | Volmer | $H^+ + e^- \rightarrow H^*$ |
| | Tafel | $H^* + H^* \rightarrow H_2$ |
| | Heyrovsky | $H^* + H^+ + e^- \rightarrow H_2$ |
| Alkaline | Volmer | $H_2O + e^- \rightarrow H^* + OH^-$ |
| | Tafel | $H^* + H^* \rightarrow H_2$ |
| | Heyrovsky | $H^* + H_2O + e^- \rightarrow H_2 + OH^-$ |
| Neutral | Volmer | $H_2O + e^- \rightarrow H^* + OH^-$ |
| | Tafel | $H^* + H^* \rightarrow H_2$ |
| | Heyrovsky | $H^* + H_2O + e^- \rightarrow H_2 + OH^-$ |

### 2.1 Hydrothermal synthesis

Strong MSI on 2D carbon-based heterogeneous catalysts through straightforward hydrothermal routes has gained widespread adoption.[86] This strategy offers several advantages, such as ease of processing, rapid synthesis, cost-effectiveness, and scalability, making it highly favorable for large-scale production.[87] More significantly, during the hydrothermal reaction, a greater abundance of oxygen-containing functional groups (–OH) are generated on the surface of the carbon substrate. These functional groups serve dual purposes: enhancing the hydrophilicity of the carbon substrate material and providing additional sites for linking with the metal active centers. Feng *et al.* synthesized a novel HER electrocatalyst of Ru and FeRu located on an amorphous and defective N-doped carbon layer (Ru-FeRu@C/NC) by a hydrothermal and pyrolysis method[71] (Fig. 2a). Through the hydrothermal and pyrolysis procedure, the synergistic interaction between the metal sites (Ru and FeRu) and the N-doped carbon matrix modulated charge distribution, reduced kinetic energy barriers, enhanced HER activity.

### 2.2 Liquid phase reduction synthesis

The liquid-phase reduction method is unnecessary for complex equipment, making it suitable for laboratory-scale synthesis.[88] Within the liquid phase, thorough mixing of reductants and reactants occurs, enabling precise control over the reaction rate by adjusting parameters such as temperature, time, and solution composition.[89] This meticulous control facilitates the manipulation of the morphology and size of metal active sites, ultimately leading to stable MSI. For example, Fu *et al.* reported PtRu alloy nanoparticles anchored on a 2D $C_2N$ matrix (PtRu@$C_2N$) HER electrocatalyst (Fig. 2b).[70] The catalyst was synthesized *via in situ* liquid $NaBH_4$ reduction of $Ru^{3+}$ and $Pt^{2+}$ on $C_2N$ layers to establish the interaction between the metal and $C_2N$ support. After annealing under an Ar atmosphere, PtRu alloy nanoparticles were successfully synthesized on $C_2N$ with stable MSI, showing extraordinary HER activity.

Table 3 Summary of the HER performance of 2D carbon-based heterogeneous catalysts prepared by several synthesis methods with the MSIs

| Electrocatalyst | $\eta_{10}$ (mV) | Electrolyte | Synthesis | Key synthesis conditions | Ref. |
|---|---|---|---|---|---|
| Ru@NC/NG | 16 mV | 1 M KOH | Small organic molecule polymerization | Stirring for 5 min, the resulting product is centrifuged | 40 |
| Ru/rGO-700 | 26 mV | 1 M KOH | Pyrolysis synthesis | 700 °C, rise rate of 10 °C $min^{-1}$ | 69 |
| PtRu@$C_2N$ | 52 mV | 0.5 M $H_2SO_4$ | Liquid phase reduction synthesis | $NaBH_4$ solution (40 mL, 10 wt% in NMP) | 70 |
| Ru-FeRu@C/NC | 23 mV | 1 M KOH | Hydrothermal synthesis | 150 °C for 24 h | 71 |
| Ru NCs/BNG | 14 mV | 1 M KOH | Pyrolysis synthesis | 300 °C, rise rate of 5 °C $min^{-1}$ for 2 h, then 700 °C in $N_2$ for 2 h, rise rate of 5 °C $min^{-1}$ | 42 |
| Ru–S/N–C | 10 mV | 1 M KOH | Pyrolysis synthesis | 900 °C for 2 h at a heating rate of 5 °C $min^{-1}$ in Ar | 44 |
| CoIr@CN-0.20 | 25 mV | 1 M KOH | Pyrolysis synthesis | 600 °C for 120 min under $N_2$ | 72 |
| Co-NC@10rGO-leaf | 220 mV | 1 M KOH | Pyrolysis synthesis | 900 °C for 2 h at a heating rate of 5 °C $min^{-1}$ under Ar | 73 |
| P@$Mn_1Co_3$-BDC($NH_2$)/NF | 102 mV | 1 M KOH | Pyrolysis synthesis | 350 °C at a rate of 2 °C $min^{-1}$ in Ar | 74 |
| CoNC/GD | 170 mV | 1 M KOH | Pyrolysis synthesis | 500 °C for 2 h at 10 °C $min^{-1}$ and then at 700 °C for 2 h under $N_2$ | 75 |
| Ru/S-rGO-24 | 14 mV at $\eta_{20}$ | 1 M KOH | Pyrolysis synthesis | 700 °C for 2 h with a heating rate of 5 °C $min^{-1}$ in $N_2$ | 46 |
| 3.0 wt%Ru/rGO | 111.7 mV | 1 M KOH | Liquid phase reduction synthesis | 1.5 g sodium borohydride, then heated to 80 °C by using a water bath | 76 |
| Ru–O/C-600 | 32 mV | 1 M KOH | Pyrolysis synthesis | 600 °C at a heating rate of 5 °C $min^{-1}$, for 3 h, at Ar/$H_2$ (5%) | 77 |
| Ru–CB[6]/rGO | 44 mV | 0.5 M $H_2SO_4$ | Hydrothermal synthesis | 150 °C for 18 h | 78 |
| Ru/p-NC | 10 mV | 1 M KOH | Pyrolysis synthesis | 850 °C for 2 h under Ar with a heating rate of 5 °C $min^{-1}$ | 48 |
| RuSA/NSG | 57.3 mV | 1 M KOH | Hydrothermal synthesis | 180 °C for 10 h | 79 |
| RuGa/N-rGO | 32 mV | 0.5 M $H_2SO_4$ | Small organic molecule polymerization | 0.5 mL of PVA aqueous solution (20 mg $mL^{-1}$) | 80 |
| Pd-NPCN | 21 mV | 1 M KOH | Small organic molecule polymerization | Stirring was continued overnight at 70 °C | 52 |
| Ru-NPCN | 11 mV | 1 M KOH | Small organic molecule polymerization | Stirring was continued overnight at 70 °C | 52 |
| Pt-NPCN | 9 mV | 1 M KOH | Small organic molecule polymerization | Stirring was continued overnight at 70 °C | 52 |
| $PtC_{60}$ | 24.3 mV | 1 M KOH | Liquid phase reduction synthesis | 200 mg $NaBH_4$ was added slowly, stirred for 12 h | 81 |
| Ru NPs/NC-900 | 19 mV | 1 M KOH | Pyrolysis synthesis | 900 °C, 1 h in $N_2$ | 54 |
| $Ru_{\Delta c\rightarrow h}$/C | 97 mV at $\eta_{50}$ | 0.5 M KOH | Pyrolysis synthesis | 750 °C for 2 h under $N_2$ | 82 |
| CoPt–CoSA@NSC | 23 mV | 1 M KOH | Pyrolysis synthesis | In $N_2$ at 800 °C for 2 h | 56 |
| NCS-CoPt | 41 mV | 0.5 M $H_2SO_4$ | Pyrolysis synthesis | 750 °C for 3 h in a tube furnace under Ar at a heating rate of 10 °C $min^{-1}$ | 38 |
| $Ni_2P$@B, N-GC | 84 mV | 1 M KOH | Liquid phase reduction synthesis | $NaBH_4$ solution (1 g per 40 mL of ethanol) | 83 |
| Cu-PDA | 104 mV | 1 M PBS | Small organic molecule polymerization | A pH of 8.5 maintained using Tris buffer (10 mg $mL^{-1}$) and NaOH solution (1 M) and stirred for 24 h | 84 |
| 3%Pd/N-PC-700 | 15 mV | 0.5 M $H_2SO_4$ | Hydrothermal synthesis | 160 °C for 8 h | 39 |
| Pt@$CoN_4$-G | 21 mV | 0.5 M $H_2SO_4$ | Pyrolysis synthesis | 400 °C for 2 h under $H_2$/Ar | 85 |

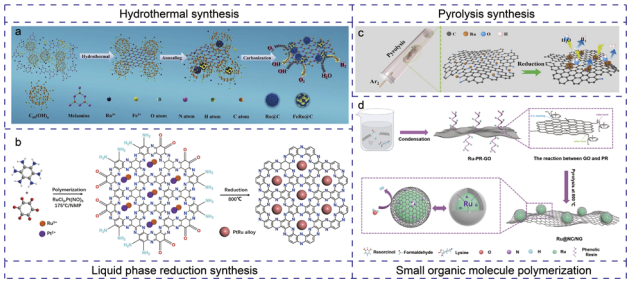


Fig. 2 Summary of the preparation approaches of 2D carbon-based heterogeneous catalysts with MSI. (a) Schematic of the hydrothermal synthesis process of the Ru-FeRu@C/NC sample. (a) adapted from Feng *et al.*,[71] Copyright 2022 Elsevier. (b) Schematic of the liquid phase reduction synthesis of PtRu@$C_2N$. (b) adapted from Fu *et al.*,[70] Copyright 2021 Elsevier. (c) Schematic diagram of pyrolysis synthesis. (c) adapted from Tian *et al.*,[69] Copyright 2022 Elsevier. (d) Schematic of the fabrication of Ru@NC/NG by small organic molecule polymerization. (d) adapted from Ma *et al.*,[40] Copyright 2022 Elsevier.

### 2.3 Pyrolysis synthesis

A common method for constructing carbon-supported catalysts is to pyrolyze small molecular precursors and metals at high temperatures in a protective or reducing atmosphere.[90,91] Pyrolysis synthesis ensures quasi-uniform carbonization within the mixed precursor, leading to the formation of intricate nanostructures.[92,93] Unlike directly loading metals onto carbon, the pyrolysis method relies on the *in situ* reduction of metal salts in the precursor mixture, allowing for the formation of more stable coordination bonds between the metal and the surrounding carbon matrix.[94] Therefore, pyrolysis represents a straightforward and highly effective approach for stable MSI on 2D carbon-based heterogeneous catalysts. For example, Tian *et al.* designed rGO supported Ru nanoparticles (Ru/rGO) with a robust Ru–O–C interface by simple heat treatment (Fig. 2c).[69] The catalyst, characterized by highly dispersed Ru nanoparticles anchored through Ru–O–C interaction, facilitated stable electron transfer pathways, accelerating the transfer of electrons. As a result, the overpotential ($\eta_{10}$) of this catalyst exhibited a mere increase of 2.5 mV even after 50 000 cycles, indicating outstanding HER activity and stability.

### 2.4 Small organic molecule polymerization

During the synthesis process, specific small organic molecules are introduced into the reaction environment, serving as a medium that facilitates the connection between the metal ions and 2D carbon substrate.[95] By these small organic molecules, the metal ions are effectively anchored onto the carbon substrate, inducing robust MSI between them.[96] For example, Ma *et al.* designed a 2D coupling hybrid comprising Ru nanoparticles within an N-doped graphene, denoted as Ru@NC/NG, by an *in situ* polymerization and pyrolysis process.[40] The N-doped carbon-encapsulated Ru nanoparticles supported by graphene are obtained *via* the pyrolysis of polymer precursors (Fig. 2d). Finally, Ru@NC/NG achieves a current density of 10 mA $cm^{-2}$ at ultralow overpotentials of 16, 24, and 72 mV in 1.0 M KOH, 0.5 M $H_2SO_4$, and 1.0 M PBS, respectively.

Primarily, these four preparation methods have effectively triggered the MSI effect in 2D carbon materials, thereby improving their HER performance. The small organic molecule polymerization approach utilizes molecules with functional groups and active sites to directly anchor metal species, thereby inducing and amplifying MSI. When the surface of the 2D carbon substrate lacks essential functional groups for anchoring metal active sites, the hydrothermal method and liquid phase reduction become involved to induce and enhance MSI. The hydrothermal method increases the active functional groups on an inert carbon matrix to anchor metal active sites, thereby stimulating and strengthening MSI. Liquid phase reduction is utilized to reduce metal precursors onto the carbon substrate through a reducing agent, thereby inducing and enhancing MSI. Subsequently, pyrolysis synthesis ensures uniform carbonization within the mixed precursor, thus further reinforcing stable MSI. Moreover, for metal single atoms, precise control over the temperature during pyrolysis synthesis is crucial. Excessively high temperatures can disrupt the structure of SACs, while low heating temperatures may result in weak MSI of SACs, leading to poor HER performance. Regarding metal nanoparticles, appropriately higher temperatures during pyrolysis synthesis enhance the crystallinity of nanoparticles and promote MSI between the nanoparticles and carbon substrate, resulting in excellent HER performance. Nevertheless, it remains imperative to avoid aggregation at ultrahigh temperatures.

## 3 2D carbon support modification for MSI regulation

Regulating MSI significantly impacts the characteristics and performances of catalysts. The design of the catalyst support is essential for optimizing the MSI. In this section, we provide a brief overview of the regulation strategies of the 2D carbon support aiming at MSI optimization, with a focus on heteroatom-doping and surface modulation, leading to outstanding HER performance.

### 3.1 Heteroatom-doping

When employed as a supporting material for metal nanoparticles, clusters and atoms, 2D carbon can undergo doping with a range of heteroatoms. Introducing heteroatoms with varying valency into the material primarily aims to adjust the electronic structure of the support, which is essential for enhancing the MSI.

**3.1.1 *Ex situ* doping.** Typically, *ex situ* doping on 2D carbon substrates with small heteroatom-containing molecules is a straightforward and dependable method. By incorporating external heteroatoms, specific sites on the carbon substrate become available for loading metal precursors, thereby facilitating the formation of a heterogeneous interface.

*3.1.1.1 Single-doping.* Single-doping refers to the introduction of only one type of heteroatom into the material, improving the catalytic activity of the catalyst. Introduction of external N atoms is a traditional strategy to enhance the binding strength

 

between the support and metal active sites. Consequently, N-doping tends to result in the formation of smaller nanoparticles and outstanding stabilities.[97] Incorporating nitrogen into a carbon matrix can vary its electronic structure, depending upon the specific position of incorporation, such as pyrrolic, pyridinic, or graphitic configurations. For example, Yang and Li *et al.* designed Co nanoparticles supported on an N doped carbon electrocatalyst (CoNC/GD), exhibiting remarkable performance in alkaline, acidic and neutral media.[75] As shown in Fig. 3a–c, CoNC/GD required overpotentials of 284, 340 and 368 mV to achieve current densities of 10 mA $cm^{-2}$, respectively. The enhanced catalytic performance of CoNC/GD was attributed to fast electron transfer within the composite. Because Co nanoparticles interacted with the alkyne rings present in the carbon support, they not only facilitated rapid electron transfer, but also enriched the electron density on the carbon shell surface.

Given the lower electronegativity of P at 2.19 compared to those of C (2.55), N (3.04), S (2.58), and O (3.5), the introduction of P into the 2D carbon support is anticipated to effectively alter the electronic configuration of the metal active sites. This modification is expected to result in intrinsically improved HER activity. For example, Guo *et al.* synthesized a 2D hybrid P-doped Mn–Co MOF electrocatalyst (P@$Mn_1Co_3$-BDC($NH_2$)) with a hierarchical porous structure.[74] Under alkaline conditions, at a current density of 10 mA $cm^{-2}$, the overpotential of P@$Mn_1Co_3$-BDC($NH_2$) was 102 mV. The hierarchical porous architecture exposed more active sites and enhanced the mass transport. By an XPS test, the peaks at 129.2, 133.4, and 134.3 eV were ascribed to P, P–C, and P–O bonds in the P 2p spectra, respectively. The ratio of P–O to P–C bonds for P@$Mn_1Co_3$-BDC($NH_2$)/NF was relatively high (1.4), demonstrating that P was successfully doped into the organic ligands. According to Co 2p spectra, the $Co^{2+}$ and $Co^{3+}$ peaks in P@$Mn_1Co_3$-BDC($NH_2$)/NF were shifted to high binding energy, compared with the other two samples. The vacant orbitals of P accommodated free electrons from Co and Mn, while excess electrons of P also filled the orbitals of Co and Mn, facilitating electron transfer and interaction. The doped P in the carboxyl groups affected the electronic environment of the metal centers, forming the P–O–M bonding that enhanced electron transfer between metal sites and the carbon matrix. Thus, the special MSI enhanced the efficiency of the electrocatalytic reactions, resulting in high HER performance.

Due to the fairly similar physical and chemical features of S and P, it is feasible to incorporate S into 2D carbon supports, which can precisely tune the electronic structures of metal active sites anchored on 2D carbon supports by adjusting the quantity of S dopants. Wang *et al.* fabricated ultrasmall Ru nanoparticles (NPs) dispersed on S-doped graphene, using a simple "one-pot" procedure.[46] The research focused on enhancing the electrocatalytic activity in heterogeneous catalysis through the MSI between S doped graphene and Ru, which increased the electron deficiency of Ru, facilitating the easy breaking of the H–OH bond (Fig. 3d and e).

By heteroatom doping on the carbon support, the empty orbital of the metal can accommodate the outer electrons of N, P and S, forming strong electron interaction. Heteroatoms connect the metal species and the carbon substrate as an electron transfer pathway. Due to the different heteroatoms, the adsorption of different metal active centers to intermediates can be optimized, thereby enhancing HER performance.

*3.1.1.2 Co-doping.* Co-doping refers to the simultaneous incorporation of two or more heterogeneous atoms into the bulk material. Research and development of co-doping is relatively more challenging, requiring a deeper understanding of the interactions between different dopant elements and their impact on material properties. Co-doping enables more precise control over the band structure of catalysts to enhance HER performance properties. Li *et al.* successfully developed S-coordinated Ru nanoclusters anchored on amorphous

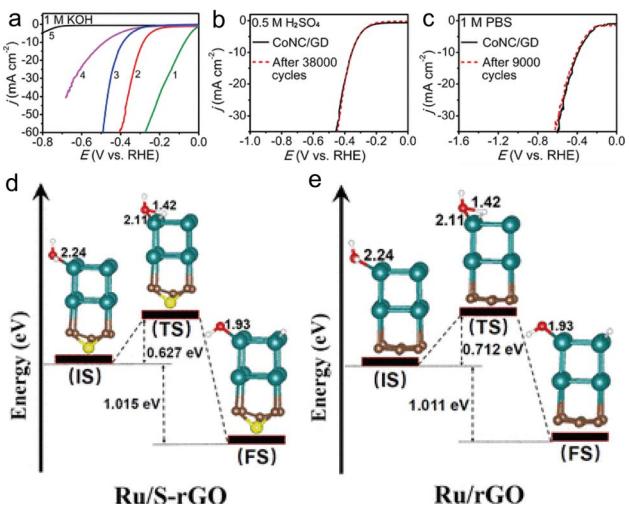


Fig. 3 Summary of single-doping for the HER. (a–c) HER polarization curves in 1 M KOH, 0.5 M $H_2SO_4$ and 1 M PBS. (a)–(c) adapted from Yang *et al.*[75] Copyright 2016 American Chemical Society. (d and e) Energy diagram of the HER on different surfaces, including the initial, intermediate, and final states of the reactants for Ru/S-rGO and Ru/rGO. The initial state, transition state, and final state are denoted as IS, TS, and FS, respectively. The atoms H, O, C, S, and Ru are pictured in white, red, brown, yellow, and light green, respectively. (d) and (e) adapted from Wang *et al.*[46] Copyright 2020 American Chemical Society.

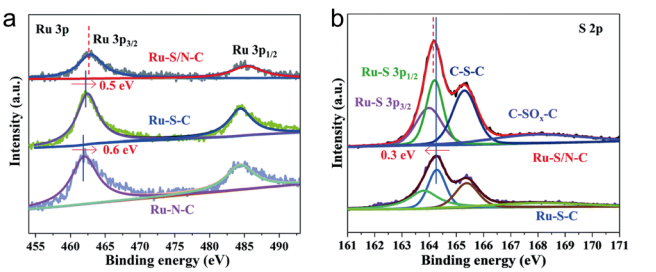


Fig. 4 Summary of co-doping for the HER. (a) XPS Ru 3p spectra of Ru–S/N–C, Ru–S–C, and Ru–N–C; (b) S 2p spectra of Ru–S/N–C and Ru–S–C; (a) and (b) adapted from Li *et al.*[44] Copyright 2021 The Royal Society of Chemistry.

nitrogen-doped carbon nanosheets (Ru–S/N–C).[44] X-ray photoelectron spectroscopy was employed to confirm the Ru–S bonds (Fig. 4a and b). The Ru $3p_{3/2}$ binding energy of Ru–S/N–C showed large positive shifts of 0.6 and 0.5 eV compared with those of Ru–N–C and Ru–S–C, respectively. Ru–S/N–C demonstrated a negative shift of 0.3 eV in its S 2p, suggesting strong interactions between S and the Ru nanoclusters induced by the N dopants on the carbon substrate. Theoretical calculations provided further confirmation that the optimized coordination and surrounding environments could enhance the adsorption energies of intermediate species on Ru through interfacial charge transfer on nitrogen-doped carbon nanosheets, resulting in accelerated reaction kinetics for the hydrogen evolution process. The Ru–S/N–C catalyst exhibited exceptional electrocatalytic performance with an ultra-small overpotential of only 10 mV at a current density of 10 mA $cm^{-2}$, along with an extremely high turnover frequency (TOF) of 2.3 $H_2$ per s at an overpotential of 50 mV for the HER. Zhang *et al.* synthesized Ru nanoclusters anchored on a boron/nitrogen-doped graphene (Ru NCs/BNG) catalyst.[42] Additionally, boron atoms were involved in coordinating with the element N, which interacted with Ru nanoclusters to promote H–OH bond cleavage, thus accelerating the water dissociation step and boosting the HER dynamics in alkaline solution.

Co-doping allows the introduction of multiple heteroatoms, which can induce synergistic effects, thereby significantly enhancing MSI. The chemical state of metal active centers can be accurately regulated by doping a variety of heterogeneous atoms, which improve HER performance.

**3.1.2 *In situ* doping.** The aforementioned doping methods are based on the carbon substrate, involving the introduction of external substances containing heteroatoms. In contrast to the aforementioned methods, certain carbon materials do not require the introduction of external sources of foreign heteroatoms. Instead, these materials possess heteroatoms in their bulk phase's chemical composition. Through processes like pyrolysis or high-temperature conversion, *in situ* doping with heteroatoms is achieved within the carbon structure.

Note that since 2D MOFs contain several kinds of heteroatoms, there is no need to introduce other heteroatom sources.[98] Compared with other 2D carbon materials, by *in situ* conversion of the heteroatom-doping in 2D MOF derivatives, the MSI between the carbon substrate derived from the MOF and metal is more effective and stable. Han *et al.* fabricated a novel hexagonal-shaped 2D ZIF-Co-L variant by adjusting the graphene oxide GO content in the reaction mixture.[73] This adjustment allowed them to achieve the hexagonal shape of the ZIF-Co-L under water-deficient conditions (Co-NC@10rGO-leaf) (Fig. 5a). The Co-NC@10rGO-leaf catalyst showed remarkable HER catalytic activity in alkaline medium, with a low overpotential ($\eta_{10}$) of 220 mV. The favorable performance was due to the MSI effects between Co nanoparticles and the highly porous N-doped 2D carbon/graphene nanosheets, which were induced by high temperature annealing. The *in situ* N doping facilitated the stable MSI. These bonds created an electron transfer pathway that enhanced the HER performance. Lin *et al.* developed a CoIr alloy supported on two-dimensional graphitic-N-doped carbon (CoIr@CN) that originated from an Ir-doped 2D Co MOF.[72] The SEM (Fig. 5b) and TEM images (Fig. 5c and d) show the morphology of 2D Ir@MOF and CoIr@CN. Owing to the strong MSI promoted by *in situ* N doping, the electron transfer between alloy nanoparticles and N-doped carbon was promoted, and the CoIr@CN demonstrated remarkable electrocatalytic performance for the HER, with low overpotentials of 70 mV at a current density of 10 mA $cm^{-2}$ in 1.0 M KOH, and only 25 mV in 0.5 M $H_2SO_4$. Fundamentally, the ultrahigh porosity, expansive surface area, and adaptable structures achieved by heteroatom doping of 2D MOFs endow upon them the potential to bind with metal active sites. Moreover, MSI is also prompted by the *in situ* heteroatom doping.

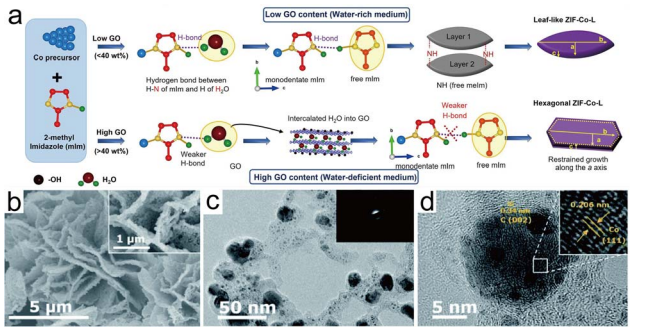


Fig. 5 Summary of the *in situ* anion doping of 2D MOF derivatives for the HER. (a) Mechanism of changes in morphology of ZIF-Co-L with the GO content. (a) adapted from Han *et al.*[73] Copyright 2021 Elsevier. (b) SEM images of CoIr@CN-0.20. (c and d) TEM and HRTEM images of CoIr@CN-0.20. (b)–(d) adapted from Lin *et al.*[72] Copyright 2022 The Royal Society of Chemistry.

*In situ* doping facilitates the direct integration of dopant atoms into the catalyst preparation, simplifying synthesis into a single step and boosting productivity. *In situ* doping enables precise control over the position, concentration, and distribution of dopant atoms during the fabrication process, enhancing MSI and promoting HER performance.

### 3.2 Surface functionalization

Surface functionalization serves as another crucial method in the design of high performance electrocatalysts. Functional groups engaged in this process can serve as electron-donors or -acceptors, effectively modifying the electronic structure of 2D carbon supports and facilitating the anchoring of metal active sites, thereby fostering effective MSI and enhancing the HER.

Over several decades, substantial advancements have been achieved in the evolution of graphene-based electrocatalysts for the HER, which is attributed to their outstanding electrical conductivity and extensive surface area. Oxygen or nitrogen-containing functional groups are frequently introduced onto graphene to regulate MSI. For example, reduced graphene oxide (rGO), a normal type of graphene with oxygen-containing functional groups on the surface, is highlighted as an excellent support material for electrochemical reactions because of its outstanding electron transport properties. The metal active sites connect with surface functional groups to form a stable

 

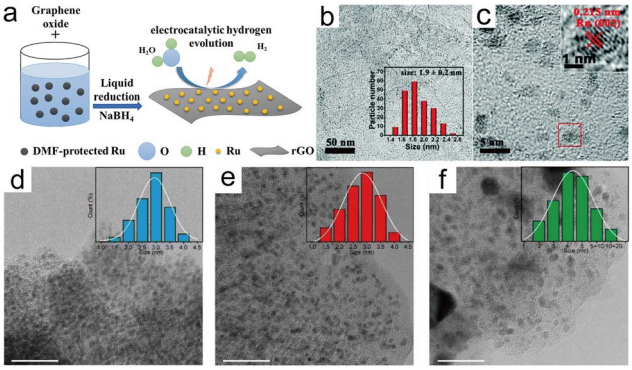


Fig. 6 Summary of surface functionalization for the HER. (a) Schematic illustration of 3.0 wt%Ru/rGO. (a) adapted from Zhu *et al.*[76] Copyright 2022 Elsevier. (b and c) TEM and HRTEM of the Ru–CB[6]/rGO. (b) and (c) adapted from Cao *et al.*[78] Copyright 2020 The Royal Society of Chemistry; HRTEM images of (d) Ru–O/C-500, (e) Ru–O/C-600 and (f) Ru–O/C-700. Scale bar: (d–f) 20 nm, 20 nm, and 20 nm, respectively. (d)–(f) adapted from Feng *et al.*[77] Copyright 2022 The Royal Society of Chemistry.

interface. Zhu *et al.* employed *N*,*N*-dimethylformamide (DMF) as an organic ligand to encapsulate Ru precursors, and subsequently deposited them onto graphene oxide, successfully preventing the agglomeration of Ru species and showing excellent HER performance[76] (Fig. 6a). Despite its advantages, the tendency of rGO nanosheets to form stacked structures arises from hydrophobic interactions and robust π-stacking forces. To counteract the formation of stacked structures and achieve the uniform anchoring of metal active sites, Cao *et al.* introduced ultrafine Ru nanoclusters anchored on thin rGO sheets.[78] The HRTEM image showed ultrathin distribution of Ru clusters on the rGO thin layers due to the robust MSI as shown in Fig. 6b and c. The dispersed Ru clusters on rGO exhibited exceptional activity with overpotentials of 44, 48 and 72 mV at 10 mA $cm^{-2}$ current density in acidic, alkaline and neutral media, respectively. This provided a strategy for the development of thin rGO-supported metal nanocluster catalysts in a broad pH range by MSI.

Apart from the traditional graphene substrate, fullerene can convert into fullerenol ($C_{60}(OH)_x$) by surface hydroxylation. Fullerenol, characterized by abundant oxygen containing functional groups, serves as a promising support for anchoring metal species. This material not only possesses the advantages of $C_{60}$ but also offers the capability to stabilize and disperse metals while precisely regulating the electronic structure of metal centers. Feng and his group designed and synthesized a 2D Ru-based nanocomposite catalyst (Ru–O/C-600) formed by $Ru^{3+}$ and a $C_{60}(OH)_n$ precursor.[77] The Ru–O/C-600 composite featured minute Ru nanoparticles, exhibiting particle sizes ranging from 2.0 to 3.5 nm as observed in HRTEM (Fig. 6d–f). These nanoparticles displayed uniform dispersion on the amorphous and defective carbon substrate. The oxygen-rich carbon matrix confinements contributed to the exposure of small particle size and even distribution, resulting in an expanded catalytic surface area that facilitated efficient electrochemical activity. Within the Ru–O/C-600 electrocatalyst, the charge transfer between Ru and O, induced by MSI, played a crucial role in regulating the electronic structure. This interaction enhanced the rate of electron transfer and optimized the intrinsic catalytic activity. Notably, the Ru–O/C-600 exhibited a low overpotential of only 32 mV at a current density of 10 mA $cm^{-2}$ in alkaline media.

Above all, surface functional groups alter the surface electronic structure of carbon substrates and provide additional binding sites for metal active sites on the surface of 2D carbon substrates to induce MSI, thereby improving HER performance and stability.

# 4 The influence of MSI on 2D carbon materials for the HER

As previously stated, the two strategies, heteroatom doping and surface functionalization, induce stable MSI to enhance HER performance. In this section, we provide a brief overview of three effects (Fig. 7) induced by MSI on 2D carbon-based catalysts, dispersion of active metal sites, establishment of efficient electron transfer pathways and electronic structure regulation by lattice strain, that can promote HER performance.

## 4.1 Dispersion of active catalytic sites

Catalysts require numerous reactive sites and high atom utilization. In the case of 2D carbon-based catalysts, the interaction between the carbon matrix and metal active sites leads to the uniform dispersion of catalytic sites, thereby enhancing the performance of the HER. Using supports with a porous open microstructure and high surface area is a wise choice, as it facilitates the rapid mass transfer of species involved in the reaction and the complete exposure of active sites by MSI (Fig. 7a). Fan *et al.* achieved a straightforward and efficient method to create hierarchically porous interconnected carbon

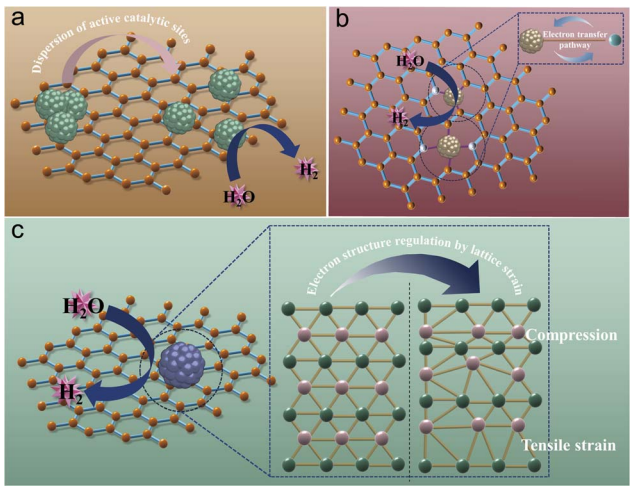


Fig. 7 Schematic of three kinds of MSI influence on 2D carbon-based materials for the HER. (a) Dispersion of active catalytic sites. (b) Construction of an electron transfer bridge between the metal and support. (c) Electronic structure regulation by lattice strain.

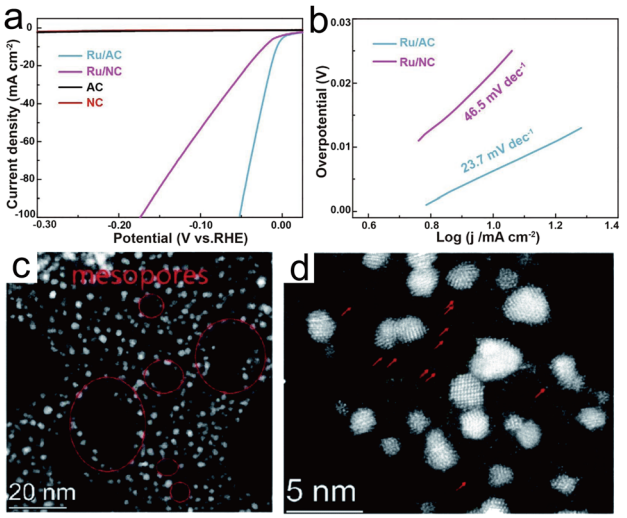


Fig. 8 The effect of dispersion of active catalytic sites induced by MSI for the HER. (a) Polarization curves in 1 M KOH. (b) Tafel plots. (a) and (b) adapted from Fan *et al.*,[50] Copyright 2021 Elsevier. (c) Representative high-angle annular dark-field scanning TEM image of Ru/p-NC. (d) A zoomed-in view of (c); red arrows signify ruthenium single atoms. (c) and (d) adapted from Xie *et al.*,[48] Copyright 2021 The Royal Society of Chemistry.

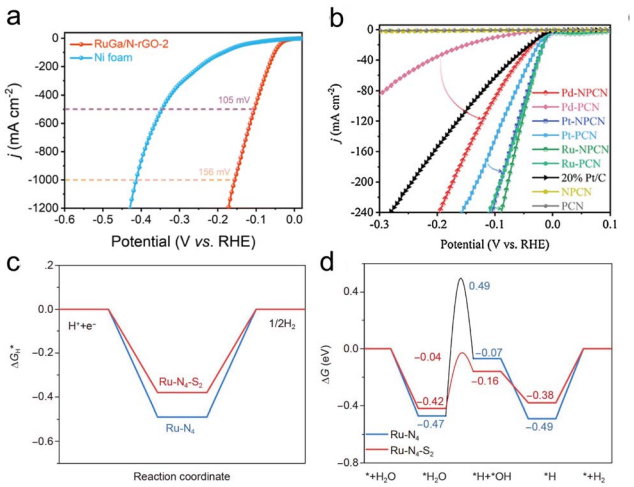


Fig. 9 The effect of electron transfer bridge induced by MSI for the HER. (a) LSV curves of RuGa/N-rGO-2 and pure Ni foam for large current density in 1.0 M KOH electrolyte. (a) adapted from Lu *et al.*,[80] Copyright 2023 The Royal Society of Chemistry. (b) Polarization curves of PCN, NPCN, 20% Pt/C, Pd/Pt/Ru-PCN and Pd/Pt/Ru-NPCN. (b) adapted from Cao *et al.*,[52] Copyright 2021 Elsevier. Calculated Gibbs free energy ($\Delta G$) diagrams of (c) hydrogen and (d) different reaction intermediates of the HER process on Ru–$N_4$ and Ru–$N_4$–$S_2$. (c) and (d) adapted from Li *et al.*,[79] Copyright 2022 Science China Press and Springer-Verlag GmbH Germany, part of Springer Nature.

nanosheets doped with oxygen and nitrogen (referred to as AC).[50] The MSI between Ru nanoparticles and the AC matrix induced uniform distribution of Ru nanoparticles. Therefore, Ru/AC exhibited an extremely small overpotential of 7 mV at 10 mA $cm^{-2}$ and high long-term durability in 1.0 M KOH (Fig. 8a and b). Xie *et al.* have also developed a high-performance single atom Ru-based electrocatalyst, termed Ru/p-NC, consisting of both Ru single atoms and Ru nanoclusters embedded in a highly porous N-doped carbon material with abundant hierarchical pores.[48] As shown in Fig. 8c and d, the high catalytic performance of Ru/p-NC was attributed to the unique porous N-doped carbon support, which not only exposed a high density of active sites, but also facilitated strong MSI with the Ru single atoms and nanoclusters, enhancing its stability. In this section, we summarize the effect of regulating the dispersion of catalytic sites on 2D carbon-based materials for the HER induced by MSI. Due to numerous surface functional groups and defects, the carbon matrix anchors the metal active site effectively, and the suitable MSI between the carbon matrix and metal active sites is conducive to the exposure of the metal active site, which leads to high-activity and long-term stability performance of the HER.

### 4.2 Construction of an electron transfer bridge between the metal and support

Establishing an electron transfer bridge between the metal and support through MSI accelerates reaction rates, because the transfer of electrons is a critical step in electrocatalytic reactions. Electron transfer within the catalyst can take place through multiple pathways, frequently involving electron-conductive channels facilitated by MSI (Fig. 7b). For example, Lu *et al.* have synthesized ordered RuGa intermetallic compounds, supported on N-doped reduced graphene oxide (RuGa/N-rGO).[80] Importantly, this catalyst exhibited remarkably low overpotentials of 105 mV and 156 mV to achieve current densities of 500 mA $cm^{-2}$ and 1000 mA $cm^{-2}$, respectively (Fig. 9a). Connecting with N-rGO, the Ru sites offered electron-rich environments to enable stronger atomic interactions, which significantly accelerated electron transfer rates and deeply reduced the energy barrier of the rate-limiting step during the HER process. Cao and Zhao *et al.* confined Pd, Pt, or Ru metal nanoparticles onto N-doped porous carbon nanosheets (NPCN).[52] The synergy between the uniformly distributed small metal nanoparticles and the N-doped carriers gave rise to an electron transport path, significantly speeded up electron transfer rates and further improved the catalytic activity of the metal-loaded porous carbon nanosheets. The Pd, Pt, and Ru supported on NPCN catalysts exhibited outstanding catalytic activity for the HER in 1.0 M KOH (21, 9 and 11 mV at 10 mA $cm^{-2}$, respectively), surpassing the performance of commercial 20 wt% Pt/C catalysts (Fig. 9b). Upon enhancing electron transfer arising from MSI between the metal and carbon substrate, the active metal sites as single atoms effectively participate in catalytic reactions, speeding up reaction rates. Li *et al.* successfully created atomically dispersed Ru single atoms that formed strong coordination bonds with dual heteroatoms, N and S, on graphene (RuSA/NSG).[79] This newly developed catalyst exhibited outstanding catalytic performance in alkaline media, with a low overpotential of 57.3 mV, enabling a current density of 10 mA $cm^{-2}$ for the HER. Through density-functional theory calculations, the customized Ru–$N_4$–$S_2$ coordination, incorporating adjacent S dopants on carbon substrates for generation of effective MSI, provided charge transfer routes, significantly expediting the sluggish kinetics of

 

the HER (Fig. 9c and d). In this section, we summarize the MSI effect of constructing an electron transfer bridge between a 2D carbon-based support and metal for the HER. There is a built-in electric field in the interface between the 2D carbon matrix and metal active sites, because of the difference of their Fermi levels, which accelerates the electron transportation. By modifying the surface of 2D carbon substrates, particularly the coordination structure of individual atoms, it becomes possible to effectively regulate MSI.

### 4.3 Electronic structure regulation by lattice strain

The interaction between the carbon substrate and metal catalytic centers commonly has a significant impact on engineering the lattice strain of metal nanoparticles and 2D carbon substrate. The atom rearrangement led by strain changes the distances, bond angles, and coordination environments of metal active sites. Therefore, the MSI is critical for optimizing the lattice strain to improve HER performance (Fig. 7c). Modifying the surface strain of the active species *via* lattice strain effects can shift the d-band center of the catalyst and optimize the adsorption energy of reaction intermediates during the HER process. Thus, Li *et al.* developed a highly efficient HER catalyst of Ru nanoparticles with lattice strain supported on nitrogen-modified carbon nanosheets.[54] By modulating the nitrogen content within the carbon supports to promote MSI, lattice strain was controlled to optimize electronic structure, resulting in outstanding HER performance. The resulting Ru NPs/NC catalyst, with an appropriate nitrogen content, demonstrated outstanding activity, as evidenced by a low overpotential of 19 mV at 10 mA $cm^{-2}$. Density functional theory calculations demonstrated that lattice strain and the Schottky junction between Ru nanoparticles and N-modified carbon modulated the d-band state and the adsorption strength of H* intermediates, thereby significantly enhancing HER activity. Similarly, Wang *et al.* illustrated a notable improvement in the catalyst for the HER by attaching platinum clusters onto two-dimensional fullerene nanosheets[81] ($PtC_{60}$). The remarkably large lattice distance (~0.8 nm) of the fullerene nanosheets caused a strong interaction between fullerene nanosheets and Pt clusters, leading to a charge redistribution at the platinum/fullerene interface. Moreover, the diffusion barriers for adsorbed hydrogen were identified to be as low as 0.22 eV on Pt, facilitating efficient hydrogen spillover among active sites, thereby augmenting the HER performance (24.3, 53.2 and 110.0 mV at 10, 50 and 150 mA $cm^{-2}$ in 1 M KOH). Due to the strong MSI, some phase transition of metal active sites may occur. Choi *et al.* explored the Ru phase transition of metastable crystal structures on a carbon support.[82] It revealed the formation of a ruthenium carbide ($RuC_X$, $X < 1$) phase during the Ru phase transition from cubic-close-packed to hexagonal-close-packed structure, which was induced by interaction between the Ru phase and carbon support. The catalyst with $RuC_X$ on the transformed hexagonal phase showed a low overpotential (97 mV) at a current density of 50 mA $cm^{-2}$ and Tafel slope of 51 mV $dec^{-1}$, which were much lower than those of other catalysts. In the case of nanoscale crystals, such phase transitions release a significant amount of energy within a confined surface area and rapidly restructure the atomic arrangement on the surface between the metal active sites and carbon support. Shen *et al.* demonstrated that lattice strain engineering induced by MSI significantly impacts HER activity, as revealed by theoretical calculations.[99] They systematically investigated the effects of lattice strain of Co,N co-decorated graphyne ($Co@N_1$-GY) on HER performance using density functional theory computations. The calculated results revealed that the stability of $Co@N_1$-GY decreased as graphyne lattice strain increased. With a transition from compressive to tensile strain, the C–Co bond length was found to linearly increase, and both the p-band center of C atoms and the d-band center of Co atoms were linearly upshifted. Specifically, the $Co@N_1$-GY catalyst employed a small tensile strain of 0.5% to achieve ideal HER performance, which was characterized by a Gibbs free energy change ($\Delta G_H^*$) of 0. In this section, the effect of lattice strain induced by MSI has been discussed. Too strong or too weak lattice strain is not suitable for the HER. Given the variety of 2D carbon substrates with adjustable lattice structures, it is rational to optimize the lattice configuration of the carbon support to regulate metal lattice strain parameters through the strength of MSI.

## 5 Conclusion and outlook

MSI have a great and profound impact on the HER performance of 2D carbon-supported electrocatalysts. In order to promote MSI on 2D carbon-supported electrocatalysts, four effective preparation strategies have been put into utilization. Two surface modulation strategies of heteroatom doping and functional group modification on 2D carbon supports facilitate and promote MSI for the HER, depending on the synthesis method. Specifically, the three MSI effects on 2D carbon-supported electrocatalysts, covering key aspects such as the distribution of metal active sites, the establishment of electron transfer pathways and electronic structure regulation by lattice strain, have been well summarized and discussed. Despite the remarkable progress achieved with the MSI of 2D carbon-based supported catalysts for the HER, there remain several unexplored research directions and future prospects that are worth further investigation.

(1) Uniform distribution of metal active sites in a high metal-loading carbon catalyst. This review discusses MSI, which maintain the dispersion of metal catalytic sites in catalysts to increase their utilization and enhance the exposure of active sites for the HER. However, maintaining the effectiveness of MSI for high loading metal active sites on 2D carbon-based materials is challenging for several reasons. Firstly, in high metal-loading catalysts, there are a large number of metal particles, making them more prone to coming into close proximity and agglomerating. Agglomeration reduces the contact area between the metal and the support, weakening the MSI. Secondly, excessive loading leads to increasingly complex interactions between metal particles, making it challenging to maintain stable MSI, which are more susceptible to interference from other factors under high-loading conditions. Therefore, it is important to explore the MSI in high-loading 2D carbon materials for HER performance.

(2) Boosting the intrinsic catalytic performance of metal active sites. The intrinsic activity is crucial for the HER, particularly in a carbon-based heterogeneous system. In general, improving the intrinsic activity requires precise regulation of the chemical state of the active site and its surrounding chemical environment. However, the chemical environment and state of active sites vary with time, temperature, and reaction conditions, making it difficult to maintain consistent and outstanding contributions from each site.

(3) Promoting structural stability. The structural stability of 2D carbon materials plays a crucial role in maintaining effective MSI. Many 2D carbon materials are susceptible to oxidation in the presence of air, leading to structural degradation and a decline in performance. This limitation restricts their application under atmospheric conditions. Due to their thin structure, 2D carbon materials often possess lower mechanical strength and toughness, making them vulnerable to mechanical stress and corrosion. This susceptibility can disrupt the initial 2D layered structure, weakening or eliminating the original interaction between the metal active sites and the carbon matrix. Moreover, during long-term catalytic stability tests, the coordination bond between the metal and the substrate can degrade, significantly hindering the electron transfer pathway and causing the aggregation of active sites, particularly in the case of single atom catalysts. Consequently, certain 2D carbon materials may lose stability during extended stability tests, necessitating measures to extend their lifespan.

(4) Scalability and commercial viability of the synthesis of 2D carbon-based heterogeneous catalysts with the MSI effect. Synthesis of 2D carbon-based heterogeneous catalysts from laboratory to industry involves two important steps, including production of 2D carbon materials and binding of metal active sites on the 2D carbon substrate. Firstly, commercial production of 2D carbon materials faces challenges such as scalability, cost, and environmental impact. Advances in production techniques like chemical vapor deposition (CVD), liquid-phase exfoliation, and mechanical exfoliation have improved the scalability and quality of these materials. Scaling up production is reducing costs through economies of scale, and investments in large-scale facilities are making 2D carbon materials more competitive. Improved resource utilization and waste management strategies are also contributing to economic viability. Environmentally, green synthesis methods and recycling strategies are addressing sustainability and safety concerns. Secondly, for binding metal active sites on 2D carbon substrates, heterogeneous catalysts with MSI effects can be synthesized using hydrothermal synthesis, liquid phase reduction, small organic molecule polymerization, and pyrolysis in labs, and show promise for commercial applications. However, low-cost, large-scale preparation methods still require further development. For instance, non-thermal synthesis methods like liquid-phase reduction and electro-reduction can be adopted and improved. Additionally, microwave and flash sintering can be used to shorten preparation time and reduce costs.

As mentioned above, the MSI effect between metal species and carbon supports is not only used in the HER, but also in the oxygen evolution reaction (OER), oxygen reduction reaction (ORR), methanol oxidation and small molecule catalytic reactions. Moreover, some studies on MSI are expanding their applications to fields such as electromagnetic shielding, energy storage, and water purification. However, more attention should be paid to the fundamental properties of electrocatalysis, particularly the MSI mechanism. Overcoming these fundamental issues and focusing on appropriate electrochemical catalysis are crucial for the commercialization of 2D carbon-based heterogeneous catalysts.

## Data availability

No primary research results, software or code have been included and no new data were generated or analysed as part of this review.

## Author contributions

Weihang Feng: conceptualization, methodology, writing – original draft. Wei Zhang: conceptualization, methodology, writing – original draft, funding acquisition. Quanying Lin: writing – original draft. Heshuang Zhang: writing – original draft. Jingyuan Qiao: writing – original draft. Linhong Xia: writing – original draft. Nosipho Moloto: writing – review & editing, supervision. Wei He: conceptualization, writing – review & editing, supervision. Zhengming Sun: funding acquisition, supervision and project administration.

## Conflicts of interest

There are no conflicts to declare.

## Acknowledgements

This work is supported by the National Key Research and Development Program of China (No. 2023YFC3009502), National Natural Science Foundation of China (No.52371134, U23A20574), Natural Science Foundation of Jiangsu Province (BK20231432), Aeronautical Science Foundation of China (2023Z015069001), and the Fundamental Research Funds for the Central Universities.

## Notes and references

1 Z. Shi, X. Zhang, X. Lin, G. Liu, C. Ling, S. Xi, B. Chen, Y. Ge, C. Tan, Z. Lai, Z. Huang, X. Ruan, L. Zhai, L. Li, Z. Li, X. Wang, G.-H. Nam, J. Liu, Q. He, Z. Guan, J. Wang, C.-S. Lee, A. R. J. Kucernak and H. Zhang, *Nature*, 2023, **621**, 300–305.

2 C. Wan, Z. Zhang, J. Dong, M. Xu, H. Pu, D. Baumann, Z. Lin, S. Wang, J. Huang, A. H. Shah, X. Pan, T. Hu, A. N. Alexandrova, Y. Huang and X. Duan, *Nat. Mater.*, 2023, **22**, 1022–1029.

3 J. Chen, C. Chen, M. Qin, B. Li, B. Lin, Q. Mao, H. Yang, B. Liu and Y. Wang, *Nat. Commun.*, 2022, **13**, 5382.

4 H. Liu, Z. Yan, X. Chen, J. Li, L. Zhang, F. Liu, G. Fan and F. Cheng, *Research*, 2020, **11**, 9068270.

 

5 H. Zhang, P. Chen, H. Xia, G. Xu, Y. Wang, T. Zhang, W. Sun, M. Turgunov, W. Zhang and Z. Sun, *Energy Environ. Sci.*, 2022, **15**, 5240–5250.
6 M. Khalid, H. A. B. Fonseca, L. G. Verga, M. Rafe Hatshan, J. L. F. Da Silva, H. Varela and S. Shahgaldi, *J. Electroanal. Chem.*, 2023, **929**, 117116.
7 J. Wang, J. Liu, B. Zhang, J. Gao, G. Liu, X. Cui, J.-X. Liu and L. Jiang, *J. Mater. Chem. A*, 2021, **9**, 22934–22942.
8 X. Zhang, Z. Luo, P. Yu, Y. Cai, Y. Du, D. Wu, S. Gao, C. Tan, Z. Li, M. Ren, T. Osipowicz, S. Chen, Z. Jiang, J. Li, Y. Huang, J. Yang, Y. Chen, C. Y. Ang, Y. Zhao, P. Wang, L. Song, X. Wu, Z. Liu, A. Borgna and H. Zhang, *Nat. Catal.*, 2018, **1**, 460–468.
9 H. Shi, Y.-T. Zhou, R.-Q. Yao, W.-B. Wan, Q.-H. Zhang, L. Gu, Z. Wen, X.-Y. Lang and Q. Jiang, *Research*, 2020, **12**, 2987234.
10 T. Xiong, B. Huang, J. Wei, X. Yao, R. Xiao, Z. Zhu, F. Yang, Y. Huang, H. Yang and M. S. Balogun, *J. Energy Chem.*, 2022, **67**, 805–813.
11 R. Boppella, J. Tan, W. Yang and J. Moon, *Adv. Funct. Mater.*, 2018, **29**, 1807976.
12 L. Yang, H. Li, Y. Yu, Y. Wu and L. Zhang, *Appl. Catal., B*, 2020, **271**, 118939.
13 C. Wu, S. Ding, D. Liu, D. Li, S. Chen, H. Wang, Z. Qi, B. Ge and L. Song, *Research*, 2020, **12**, 5860712.
14 D. Voiry, H. Yamaguchi, J. Li, R. Silva, D. C. B. Alves, T. Fujita, M. Chen, T. Asefa, V. B. Shenoy, G. Eda and M. Chhowalla, *Nat. Mater.*, 2013, **12**, 850–855.
15 Y. Zang, D.-Q. Lu, K. Wang, B. Li, P. Peng, Y.-Q. Lan and S.-Q. Zang, *Nat. Commun.*, 2023, **14**, 1792.
16 Y. Qiu, Y. Rao, Y. Zheng, H. Hu, W. Zhang and X. Guo, *InfoMat*, 2022, **4**, 12326.
17 T. Xiong, Z. Zhu, Y. He, M. S. Balogun and Y. Huang, *Small Methods*, 2023, **7**, 2201472.
18 F. Yang, T. Xiong, P. Huang, S. Zhou, Q. Tan, H. Yang, Y. Huang and M. S. Balogun, *Chem. Eng. J.*, 2021, **423**, 130279.
19 Y. Wang, D. Chen, J. Zhang, M. S. Balogun, P. Wang, Y. Tong and Y. Huang, *Adv. Funct. Mater.*, 2022, **32**, 2112738.
20 B. Chen, Y.-F. Jiang, H. Xiao and J. Li, *Chin. J. Catal.*, 2023, **50**, 306–313.
21 Z. Chen, W. Chen, L. Zheng, T. Huang, J. Hu, Y. Lei, Q. Yuan, X. Ren, Y. Li, L. Zhang, S. Huang, S. Ye, Q. Zhang, X. Ouyang, X. Sun and J. Liu, *Sci. China: Chem.*, 2022, **65**, 521–531.
22 X. Qin, O. Ola, J. Zhao, Z. Yang, S. K. Tiwari, N. Wang and Y. Zhu, *Nanomaterials*, 2022, **12**, 1806.
23 P. Trogadas, T. F. Fuller and P. Strasser, *Carbon*, 2014, **75**, 5–42.
24 H. Yu, L. Hui, Y. Xue, Y. Liu, Y. Fang, C. Xing, C. Zhang, D. Zhang, X. Chen, Y. Du, Z. Wang, Y. Gao, B. Huang and Y. Li, *Nano Energy*, 2020, **72**, 104667.
25 T. Lu and H. Wang, *Nano Res.*, 2022, **15**, 9764–9778.
26 K. Ma, J. Wu, X. Wang, Y. Sun, Z. Xiong, F. Dai, H. Bai, Y. Xie, Z. Kang and Y. Zhang, *Angew. Chem., Int. Ed.*, 2022, **61**, 202211094.
27 Y. Gao, Y. Xue, T. Liu, Y. Liu, C. Zhang, C. Xing, F. He and Y. Li, *Adv. Sci.*, 2021, **8**, 2102777.
28 G. Alemany-Molina, M. Navlani-Garcia, J. Juan-Juan, E. Morallon and D. Cazorla-Amoros, *J. Colloid Interface Sci.*, 2024, **660**, 401–411.
29 J. Cheng, X. Yang, X. Yang, R. Xia, Y. Xu, W. Sun and J. Zhou, *Fuel Process. Technol.*, 2022, **229**, 107174.
30 M. Han, J. Yang, J. Jiang, R. Jing, S. Ren and C. Yan, *J. Colloid Interface Sci.*, 2021, **582**, 1099–1106.
31 L. He, J. Liu, Y. Liu, B. Cui, B. Hu, M. Wang, K. Tian, Y. Song, S. Wu, Z. Zhang, Z. Peng and M. Du, *Appl. Catal., B*, 2019, **248**, 366–379.
32 Y. Liu, J. Wu, Y. Zhang, X. Jin, J. Li, X. Xi, Y. Deng, S. Jiao, Z. Lei, X. Li and R. Cao, *ACS Appl. Mater. Interfaces*, 2023, **15**, 14240–14249.
33 D. Zhao, Z. Li, X. Yu, W. Zhou, Q. Wu, Y. Luo, N. Wang, A. Liu, L. Li and S. Chen, *Chem. Eng. J.*, 2022, **450**, 138524.
34 D. Li, Y. Liu, Z. Liu, J. Yang, C. Hu and L. Feng, *J. Mater. Chem. A*, 2021, **9**, 15019–15026.
35 S. Liu, L. Dai, Y. Qu, Y. Qiu, J. Fan, X. Li, Q. Zhang and X. Guo, *Mater. Chem. Front.*, 2021, **5**, 6648–6658.
36 H. Song, M. Wu, Z. Tang, J. S. Tse, B. Yang and S. Lu, *Angew. Chem., Int. Ed.*, 2021, **60**, 7234–7244.
37 H. Wang, P. Yang, D. Liu, M. Yu, B. Zhou, Y. Zhang, Z. Xiao, W. Xiao, Z. Wu and L. Wang, *J. Colloid Interface Sci.*, 2023, **651**, 686–695.
38 Q. Xie, J. Li, K. Wang, S. Li, W. Xu, Y. Wang, L. Lei, S. Li, L. Zhuang and Z. Xu, *Mater. Chem. Front.*, 2023, **7**, 1607–1616.
39 L. Shao, Y. Sheng, Y. Li, C. Jiang, Y. Li, S. Zhang and J. Wang, *Chem. Eng. Sci.*, 2024, **291**, 119951.
40 J. Ma, J. Wang, J. Liu, X. Li, Y. Sun and R. Li, *J. Colloid Interface Sci.*, 2022, **620**, 242–252.
41 H. Cai, L. Wang, W. Liu, X. Zhang, B. Chen, P. Mao, J. Fang, R. Gao and C. Shi, *Small*, 2023, **19**, 2207146.
42 S. Ye, F. Luo, T. Xu, P. Zhang, H. Shi, S. Qin, J. Wu, C. He, X. Ouyang, Q. Zhang, J. Liu and X. Sun, *Nano Energy*, 2020, **68**, 104301.
43 C. Sun, Y. Tan, Y. Wen, Y. Yang, F. Guo, H. Huang, W. Ma and S. Cheng, *Nanoscale*, 2024, **16**, 4014–4024.
44 C.-F. Li, J.-W. Zhao, L.-J. Xie, Y. Wang, H.-B. Tang, L.-R. Zheng and G.-R. Li, *J. Mater. Chem. A*, 2021, **9**, 12659–12669.
45 M. Wu, R. Zhang, C. Li, X. Sun, G. Chen, L. Guo, K. Zheng and X. Sun, *Mater. Chem. Front.*, 2023, **7**, 4918–4927.
46 X. Sun, X. Gao, J. Chen, X. Wang, H. Chang, B. Li, D. Song, J. Li, H. Li and N. Wang, *ACS Appl. Mater. Interfaces*, 2020, **12**, 48591–48597.
47 X. Yu, X. Liu, J. Zhao, M. Xue, H. Shi, C. Jiang, J. Liu, Y. Xue, F. Gao, X. Zhong, Z. Yao and J. Wang, *Chem. Eng. Sci.*, 2024, **286**, 119652.
48 Y. Li, H. Liu, B. Li, Z. Yang, Z. Guo, J.-B. He, J. Xie and T.-C. Lau, *J. Mater. Chem. A*, 2021, **9**, 12196–12202.
49 Y. Chen, K. Yue, J.-W. Zhao, Z. Cai, X. Wang and Y. Yan, *Chem. Eng. J.*, 2023, **466**, 143097.
50 Q. Luo, Q. Chen, Y. Wang, Y. Long, W. Jiang and G. Fan, *Chem. Eng. J.*, 2021, **420**, 130483.
51 V. H. Do, Y. Li, P. Prabhu, W. Xie, P. Kidkhunthod, H. Wang, G. Wang and J. M. Lee, *Adv. Funct. Mater.*, 2023, **33**, 2302297.
52 W. H. Li, Z. Zhang, Z. H. Zhou, L. J. Yang, X. C. Zhao and W. Cao, *J. Colloid Interface Sci.*, 2022, **605**, 528–536.

53 P. Yang, F. Liu, X. Zang, L. Xin, W. Xiao, G. Xu, H. Li, Z. Li, T. Ma, J. Wang, Z. Wu and L. Wang, *Adv. Energy Mater.*, 2024, **14**, 2303384.
54 Z. Jiang, S. Song, X. Zheng, X. Liang, Z. Li, H. Gu, Z. Li, Y. Wang, S. Liu, W. Chen, D. Wang and Y. Li, *J. Am. Chem. Soc.*, 2022, **144**, 19619–19626.
55 L. Zhao, Z. Tao, M. You, H. Xiao, S. Wang, W. Ma, Y. Huang, B. He and Q. Chen, *Adv. Sci.*, 2024, 2309750.
56 Y. Li, X. Liu, S. Xue, A. Liu, S. Wen and S. Chen, *Small*, 2023, **19**, 2302170.
57 Y. Pi, Z. Qiu, Y. Sun, H. Ishii, Y. F. Liao, X. Zhang, H. Y. Chen and H. Pang, *Adv. Sci.*, 2023, **10**, 2206096.
58 L. Zong, F. Lu, P. Li, K. Fan, T. Zhan, P. Liu, L. Jiang, D. Chen, R. Zhang and L. Wang, *Adv. Mater.*, 2024, e2403525, DOI: 10.1002/adma.202403525.
59 C. Yan, Y. L. Liu, Q. Zeng, G. G. Wang and J. C. Han, *Adv. Funct. Mater.*, 2022, **33**, 2210837.
60 L. Tan, C. Nie, Z. Ao, H. Sun, T. An and S. Wang, *J. Mater. Chem. A*, 2021, **9**, 17–33.
61 D. Thanh Tran, T. Kshetri, N. Dinh Chuong, J. Gautam, H. Van Hien, L. Huu Tuan, N. H. Kim and J. H. Lee, *Nano Today*, 2018, **22**, 100–131.
62 D. Cao, J. Wang, H. Xu and D. Cheng, *Small*, 2021, **17**, 2101163.
63 Y. Feng, W. Feng, J. Wan, J. Chen, H. Wang, S. Li, T. Luo, Y. Hu, C. Yuan, L. Cao, L. Feng, J. Li, R. Wen and J. Huang, *Appl. Catal., B*, 2022, **307**, 121193.
64 Y. Liu, N. Chen, W. Li, M. Sun, T. Wu, B. Huang, X. Yong, Q. Zhang, L. Gu, H. Song, R. Bauer, J. S. Tse, S. Q. Zang, B. Yang and S. Lu, *SmartMat*, 2021, **3**, 249–259.
65 Q. Pan, X. Chen, H. Liu, W. Gan, N. Ding and Y. Zhao, *Mater. Chem. Front.*, 2021, **5**, 4596–4603.
66 A. H. Shah, Z. Zhang, Z. Huang, S. Wang, G. Zhong, C. Wan, A. N. Alexandrova, Y. Huang and X. Duan, *Nat. Catal.*, 2022, **5**, 923–933.
67 X. Wang, Z. Yang, W. Si, X. Shen, X. Li, R. Li, Q. Lv, N. Wang and C. Huang, *Carbon*, 2019, **147**, 9–18.
68 L. Qi, Y.-Q. Su, Z. Xu, G. Zhang, K. Liu, M. Liu, E. J. M. Hensen and R. Y.-Y. Lin, *J. Mater. Chem. A*, 2020, **8**, 22974–22982.
69 Y. Yang, D. Wu, Y. Yu, J. Li, P. Rao, C. Jia, Z. Liu, Q. Chen, W. Huang, J. Luo, P. Deng, Y. Shen and X. Tian, *Chem. Eng. J.*, 2022, **433**, 134421.
70 C. Li, L. Zhang, Y. Zhang, Y. Zhou, J. Sun, X. Ouyang, X. Wang, J. Zhu and Y. Fu, *Chem. Eng. J.*, 2022, **428**, 131085.
71 W. Feng, Y. Feng, J. Chen, H. Wang, Y. Hu, T. Luo, C. Yuan, L. Cao, L. Feng and J. Huang, *Chem. Eng. J.*, 2022, **437**, 135456.
72 W. Chen, Y. Xie, X. Gao, L. Li and Z. Lin, *J. Mater. Chem. A*, 2022, **10**, 15543–15553.
73 S. Gayathri, P. Arunkumar, R. Bose, A. Alfantazi and J. H. Han, *Chem. Eng. J.*, 2021, **426**, 131270.
74 R. Tian, F. Wang, C. Zou, Z. Pei, X. Guo and H. Yang, *J. Alloys Compd.*, 2023, **933**, 167670.
75 Y. Xue, J. Li, Z. Xue, Y. Li, H. Liu, D. Li, W. Yang and Y. Li, *ACS Appl. Mater. Interfaces*, 2016, **8**, 31083–31091.
76 Y. Feng, S. Zhang, L. Zhu, G. Li, N. Zhao, H. Zhang and B. H. Chen, *Int. J. Hydrogen Energy*, 2022, **47**, 39853–39863.
77 W. Feng, Y. Feng, Y. He, J. Chen, H. Wang, T. Luo, Y. Hu, C. Yuan, L. Cao, L. Feng and J. Huang, *Inorg. Chem. Front.*, 2022, **9**, 4151–4159.
78 Z. Gong, D. Wu, M. Cao, C. Zhao and R. Cao, *Chem. Commun.*, 2020, **56**, 9392–9395.
79 Z. Zhang, L. Ni, H. Liu, Z.-L. Zhao, X.-Z. Yuan and H. Li, *Sci. China: Chem.*, 2022, **65**, 611–618.
80 H. Zhang, C. Cheng, J. Zhou, C. Ma, P. Shi, H. Wu, P. Yin, W. Cao, J. Xia, L. Zhu, A.-L. Wang and Q. Lu, *J. Mater. Chem. A*, 2023, **11**, 10328–10336.
81 J. Chen, M. Aliasgar, F. B. Zamudio, T. Zhang, Y. Zhao, X. Lian, L. Wen, H. Yang, W. Sun, S. M. Kozlov, W. Chen and L. Wang, *Nat. Commun.*, 2023, **14**, 1711.
82 J. Kim, H. J. Kim, B. Ruqia, M. J. Kim, Y. J. Jang, T. H. Jo, H. Baik, H. S. Oh, H. S. Chung, K. Baek, S. Noh, M. Jung, K. J. Kim, H. K. Lim, Y. S. Youn and S. I. Choi, *Adv. Mater.*, 2021, **33**, 2105248.
83 C. Lyu, J. Cheng, Y. Yang, W. M. Lau, N. Wang, Q. Wu and J. Zheng, *J. Colloid Interface Sci.*, 2023, **651**, 93–105.
84 D. Kim, J. An, S. Surendran, J. Lim, H. Y. Jeong, S. Im, J. Young Kim, K. T. Nam and U. Sim, *J. Colloid Interface Sci.*, 2023, **650**, 1406–1414.
85 M. Zhang, H. Li, J. Chen, F. X. Ma, L. Zhen, Z. Wen and C. Y. Xu, *Adv. Funct. Mater.*, 2023, **33**, 2303189.
86 K. Chhetri, A. Muthurasu, B. Dahal, T. Kim, T. Mukhiya, S. H. Chae, T. H. Ko, Y. C. Choi and H. Y. Kim, *Mater. Today Nano*, 2022, **17**, 100146.
87 T. Feng, Z. Cui, P. Guo, X. Wang, J. Li, X. Liu, W. Wang and Z. Li, *Int. J. Hydrogen Energy*, 2023, **48**, 15522–15532.
88 Y. Fang, Y. Xue, L. Hui, H. Yu, Y. Liu, C. Xing, F. Lu, F. He, H. Liu and Y. Li, *Nano Energy*, 2019, **59**, 591–597.
89 W. Wang, Y. Wu, Y. Lin, J. Yao, X. Wu, C. Wu, X. Zuo, Q. Yang, B. Ge, L. Yang, G. Li, S. Chou, W. Li and Y. Jiang, *Adv. Funct. Mater.*, 2021, **32**, 2108464.
90 M. Lao, G. Zhao, P. Li, T. Ma, Y. Jiang, H. Pan, S. X. Dou and W. Sun, *Adv. Funct. Mater.*, 2021, **31**, 2100698.
91 W. Tang, L. Zhang, H. Huang, Y. Luo, C. Dong, D. Zhou, A. Li, W. Dong, G. Wang and Y. He, *Mater. Today Chem.*, 2023, **33**, 101666.
92 A. Salah, L. Zhang, H. Tan, F. Yu, Z. Lang, N. Al-Ansi and Y. Li, *Adv. Energy Mater.*, 2022, **12**, 2200332.
93 W. Yan, H. Ma, X. Zhao, Y. Zhang, P. Vishniakov, X. Wang, X. Zhong, Z. Hong, M. Y. Maximov, L. Song, S. Peng and L. Li, *Small*, 2023, **19**, 2208270.
94 Q. Wu, H. Li, Y. Zhou, S. Lv, T. Chen, S. Liu, W. Li and Z. Chen, *Inorg. Chem.*, 2022, **61**, 11011–11021.
95 L. Hui, Y. Xue, B. Huang, H. Yu, C. Zhang, D. Zhang, D. Jia, Y. Zhao, Y. Li, H. Liu and Y. Li, *Nat. Commun.*, 2018, **9**, 5309.
96 T. Luo, J. Huang, Y. Hu, C. Yuan, J. Chen, L. Cao, K. Kajiyoshi, Y. Liu, Y. Zhao, Z. Li and Y. Feng, *Adv. Funct. Mater.*, 2023, **33**, 2213058.
97 X. Zhang, J. Li, L. Yan, S. Huang, P. Zhang, Z. Peng, L. Zheng and C. Zhao, *Appl. Sur. Sci.*, 2021, **559**, 149978.
98 Z. Xu, C.-L. Yeh, J.-L. Chen, J. T. Lin, K.-C. Ho and R. Y.-Y. Lin, *ACS Sustain. Chem. Eng.*, 2022, **10**, 11577–11586.
99 X. Gao, Y. Zhou, Y. Tan, S. Liu, Z. Cheng and Z. Shen, *Phys. Chem. Chem. Phys.*, 2020, **22**, 2457–2465.

 